Chapter 1

Fundamental Concept for the Theory, Dynamics and Applications of MRI

1

Fundamental Concept for the Theory, Dynamics and Applications of MRI

Abhishek Gupta, Timothy Stait-Gardner, Bahman Ghadirian
and William S. Price[1]

*Nanoscale Organisation and Dynamics Group, School of Science and Health,
University of Western Sydney, Australia*

1.1 Introduction

Since its inception in 1973,[1] magnetic resonance imaging (MRI) has been a powerful diagnostic tool which is now routinely used in clinical medicine. Contrary to other non-invasive imaging techniques such as X-ray computed tomography and positron emission tomography, MRI does not use harmful ionizing radiation. Also, MRI offers much better soft-tissue contrast. MRI possesses many contrast generating mechanisms which are sensitive to various tissue parameters and ultimately provide information-rich images.

---

[1] Author for correspondence. Email: w.price@uws.edu.au

'MRI' is a branch of nuclear magnetic resonance (NMR), but the word 'nuclear' is generally omitted to avoid confusion with ionizing radiation.[2, 3] In simple terms, MRI is the use of one or more magnetic gradients to provide a well-defined spatial dependence to NMR observables. As will be considered further below, the recorded NMR signals are then reconstructed to form a spatial image.[4]

Some fundamental NMR concepts are discussed in the next section followed by a brief description of the theory, contrast and applications of MRI. Although an attempt has been made to make this chapter self-complete, due to the vast subject matter the coverage is nevertheless superficial. Therefore, the reader is suggested to refer to other texts[4-11] for further information.

1.2 Preliminary Concepts

1.2.1 Nuclear Spin and Magnetic Moment

All atomic nuclei have four important properties: mass, electric charge, magnetism and spin. Mass and electric charge are responsible for the physical and chemical properties of matter whereas the latter two properties form the basis of NMR (and hence MRI). Atomic nuclei can act as small bar magnets when placed in an external magnetic field. Spin is an intrinsic quantum mechanical property which is difficult to visualize, but simplistically can be described as atomic nucleus spinning about its own axis. This is associated with an inherent angular momentum, called the spin angular momentum, I, which gives rise to a magnetic moment μ, related to I by:

$$\boldsymbol{\mu} = \gamma \mathbf{I} \tag{1.1}$$

where the proportionality constant, γ, is the gyromagnetic ratio (rad s^{-1} T^{-1}). Equation (1.1) indicates that only the spins[2] with $I \neq 0$ possess a magnetic moment and are thus 'NMR active'. Most elements have at least one NMR active isotope. Commonly used isotopes in NMR studies include ^{13}C, ^{15}N, ^{17}O, and ^{19}F, however MRI is mainly performed with ^{1}H because of its high natural abundance (i.e., 99.9%), high NMR sensitivity (high gyromagnetic ratio) and high concentration in molecules in the body (i.e., water, fat and other organic molecules).

Larmor Precession and Net Magnetization
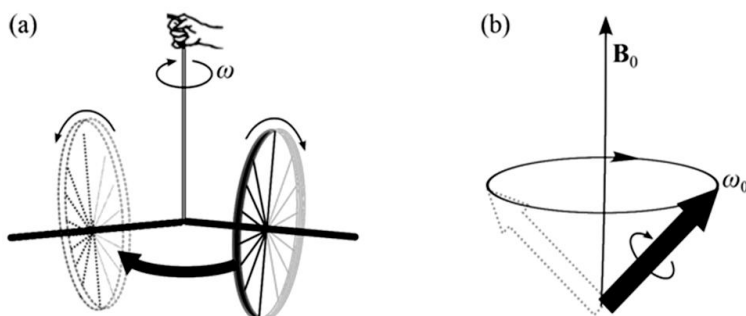
Figure 1.1 *(a) A bicycle wheel spinning about its own axis will start precessing if hung by one end of its axle. (b) Similarly, when placed in an external magnetic field (B_0), a nuclear spin starts precessing about the direction of B_0 with the Larmor precessional frequency, ω_0.*

MRI involves the application of a strong static magnetic field, B_0, to the spins. To understand how spins behave in the presence of B_0, it is useful to discuss the following analogy. Imagine a bicycle wheel hung by one end of its axle as shown in Figure 1.1 (a). If the wheel is not spinning, it will simply fall down under the effect of gravity. But if the wheel is spinning, it will instead start revolving around the fixed end while rotating about its axle. This simultaneous

---

[2] In NMR jargon, atomic nuclei are often denoted as 'nuclear spins' or 'spins'.

rotating revolving motion is called precession. This is precisely how (the magnetic property of) a nuclear spin interacts with the external magnetic field. Instead of flipping towards the magnetic field, it starts precessing about it (Figure 1.1 (b)). The angular frequency of precession, ω_0, is referred to as Larmor frequency (i.e., the resonance frequency) and its magnitude is dependent on the external magnetic field strength as:

$$\omega_0 = \gamma B_0. \tag{1.2}$$

A small digression: the magnetic field experienced by a nucleus is not necessarily exactly that of the externally applied magnetic field. The electron shells surrounding a nucleus 'shield' the nucleus from the magnetic field and thus the Larmor frequency is slightly changed by the local chemical environment ('the chemical shift'). Thus, for example, the –OH proton of methanol will resonate at a slightly different frequency than the $-CH_3$ protons. Typically though these are extremely small perturbations to the resonance frequency with the values normally being within a few parts per million of ω_0.[12, 13]

Of course, as is the case with the spinning bicycle wheel, the nuclear spin does try to align its magnetic moment with the external magnetic field to minimise the energy of magnetic interaction between them as given by:

$$E = -\mathbf{\mu} \cdot \mathbf{B}_0. \tag{1.3}$$

However, in the case of protons, it turns out that the average thermal energy associated with the absolute temperature, kT (where k is the Boltzmann's constant), is much higher than E. For example, using Equations (1.1) and (1.3), the difference in the energy of magnetic interaction of a proton between the two spin states (aligned and anti aligned with external magnetic field) can be calculated to be 4.23×10^{-26} J at 1.5 T magnetic field strength (same as that of

most clinical MRIs). Whereas, the thermal energy associated with the proton at physiological temperatures (37 ℃ or 310.15 K) is 4.28×10^{-21} J, about 10^5 times larger than E. This implies that even in the presence of the magnetic field, the spins are mostly randomly oriented with only a small preference towards the direction of the applied field. But since there are an extraordinary number of nuclei even in the smallest sample (e.g., a mg of tissue), this statistically tiny alignment can conduce to a net macroscopic magnetisation, M_0 (Figure 1.2), referred to as the thermal equilibrium value of the net magnetisation.
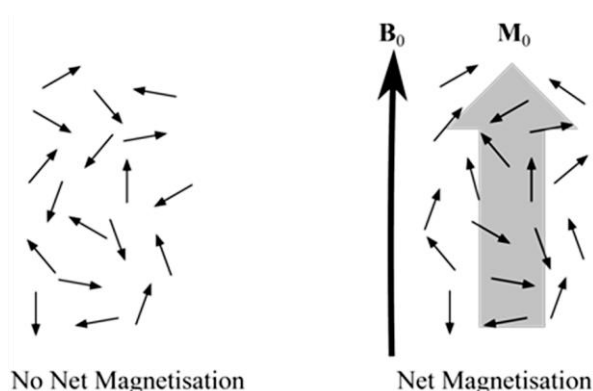
Figure 1.2 A schematic representation of nuclear spins before (left) and after (right) the application of an external magnetic field, B_0. In the absence of B_0, the magnetic moments of nuclear spins are randomly oriented resulting in no net magnetisation. Whereas, in the presence of B_0, there is a slight preference of magnetic moments to align with B_0 resulting in a small net magnetisation, M_0.

1.2.2 Radiofrequency Pulse and Signal Detection

To extract information from the sample, it is necessary to be able to detect the net magnetisation. Only the component of the net magnetisation that is oriented perpendicular to B_0 (i.e., transverse magnetisation) is detectable. Thus, an NMR (or MRI) experiment begins by nutating M_0 away from B_0 using a perpendicular magnetic field, B_1, oscillating at the Larmor frequency for a short time. Since the Larmor frequencies at most practical magnetic field strengths lie within the

radio-frequency (rf) range (3 kHz – 300 GHz), this short burst of an oscillating perpendicular magnetic field is termed a radio-frequency pulse (rf pulse). Note that MRI can also be performed in the earth's magnetic field which results in the Larmor frequencies of approximately 2 kHz for protons, lying in the ultra-low frequency or audio frequency range (300 Hz – 3 kHz).[14] However, since clinical MRI and cryogenically cooled research grade MRIs all have Larmor frequencies in the radio-frequency range, the term 'rf pulse' is generally accepted as standard. The resonance between the rf pulse and the Larmor frequency of the nuclei (i.e. $\omega_{rf} = \omega_0$) ensures that the net magnetisation receives a continuous push (actually a nutation) towards the transverse plane. The angle by which the net magnetisation is rotated (rotation angle) depends on the strength and duration of the rf pulse. It is common in NMR to name the rf pulse based on the rotation angle. For example, an rf pulse which rotates the magnetisation by 180 ° is called a π pulse or a 180 ° pulse.

Since there are two precessions involved (one about B_0 and one about B_1) during the application of an rf pulse, it is much simpler to visualize this effect in a reference frame rotating at the frequency of the rf pulse[3], otherwise known as the rotating frame of reference (RFR). In the RFR, at thermal equilibrium, the spins precessing about B_0 will appear stationary and B_0 can be ignored as its effect has already been accounted for in the rotation of the reference frame. Also, the rf pulse will appear static and the spins will appear as if only precessing about B_1 at a frequency $\omega_{rf} = \gamma B_1$ (Figure 1.3). In this chapter, RFR is represented by italiced axes (x, y, z) and laboratory frame by non-italiced axes (x, y, z).

---

[3] In many texts, RFR is arbitrarily chosen to be rotating at the Larmor frequency instead of the rf pulse frequency. Although in the present case it would not make a difference since they are both equal, in the quantum mechanical description of MRI it is more useful to describe $\omega_{rfr} = \omega_{rf}$ to account for the very small difference between ω_{rf} and ω_0 at the resonance condition.
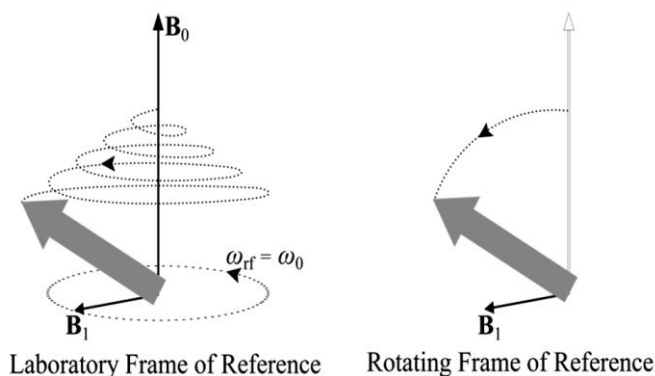
Figure 1.3 *The effect of an rf pulse on the net magnetisation in the laboratory and rotating frame of references. In the laboratory frame of reference, the two simultaneous precessions about the external magnetic field, B_0, and oscillating magnetic field B_1 makes the overall motion of the net magnetisation appear as a spiral. This can be simplified by using a reference frame rotating at the frequency of the rf pulse (or Larmor frequency), called the rotating frame of reference (RFR). In RFR, the effect of B_0 can be ignored and B_1 appears stationary. Thus, the net magnetisation appears to be precessing about B_1 only.*

After the rf pulse is turned off, the net magnetisation, now in the transverse plane, continues its usual precession about B_0. This precessing magnetisation generates a changing magnetic field which induces an oscillating electric current via Faraday induction in a nearby receiver coil. The induced current is then amplified and digitized by an analogue-to-digital converter to give an NMR signal known as the free induction decay (FID). The FID is an exponentially decaying sinusoidal signal in the time domain. As can be seen from Figure 1.4, it is very hard to deduce the Larmor frequencies of nuclei in differing chemical environments (such as situated in or near different functional groups) with different resonance frequencies from the FID. To resolve this, the FID is Fourier transformed to the frequency domain (i.e., an NMR spectrum) in which each exponentially decaying signal is converted to a Lorentzian shaped peak. In an NMR spectrum, the Larmor frequencies can be easily identified by the corresponding peaks (Figure 1.4).[15, 16]
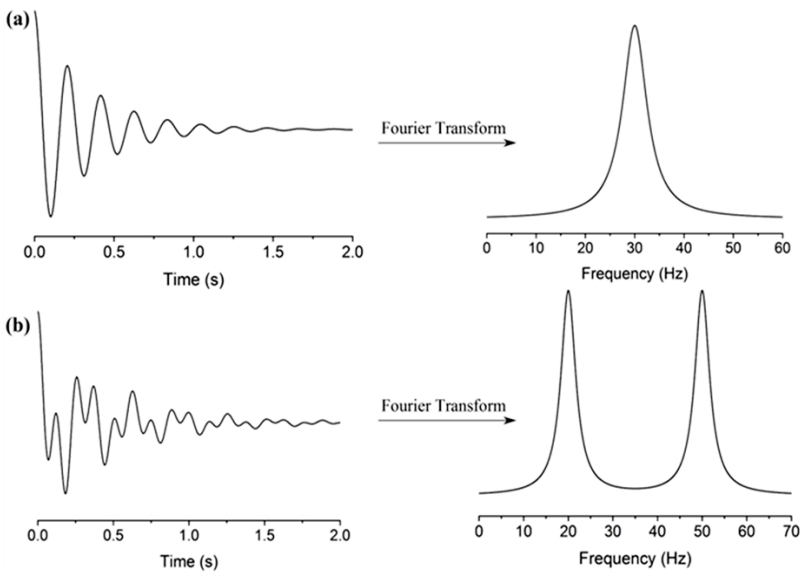
Figure 1.4 *Simulated free induction decays (left) and their NMR spectra (right) obtained by applying the Fourier transforms. The offset Larmor frequencies were set to (a) 30 Hz and (b) 30 and 50 Hz (a situation where either different nuclei are present or the same nuclei are present in two different environments). T_2 was set to 2s in both cases. Whilst it is hard to deduce directly the Larmor frequencies of the nuclei contributing to the FID signal (time domain), the frequencies can be easily identified by the corresponding peaks in the NMR spectrum (frequency domain).*

1.2.3 Relaxation

After the rf pulse, the net magnetisation returns to its equilibrium position by a process known as spin relaxation. This includes the reduction of the transverse magnetisation to zero (transverse relaxation) and the longitudinal magnetisation back to its equilibrium value (longitudinal relaxation).[9, 11] The two processes are outlined in Figure 1.5 and briefly discussed below. Note that for the sake of discussion, B_0 is assumed to be directed along the z-axis, although depending on magnet construction it could be along any direction. Indeed in clinical whole body magnets it is generally taken as being along x.
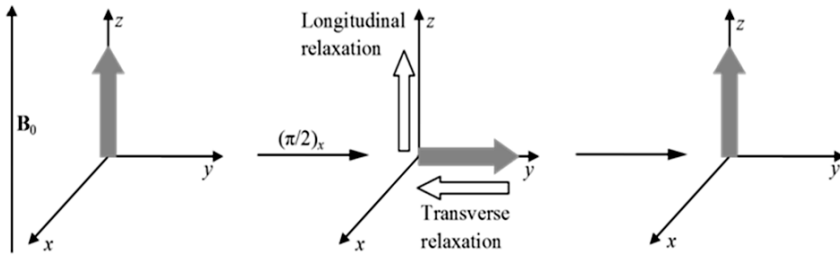
Figure 1.5 *A schematic representation of the relaxation process. The net magnetisation is along the direction of the applied magnetic field, B_0, at equilibrium. The π/2 rf pulse rotates it to the x-y plane. Relaxation drives the transverse magnetisation to zero (transverse relaxation) and the longitudinal magnetisation to its equilibrium value (longitudinal relaxation).*

(1) Longitudinal Relaxation

Longitudinal relaxation is also known as spin-lattice relaxation or somewhat erroneously, T_1 relaxation. At the microscopic scale, it refers to the movement of spin populations back to their Boltzmann distribution values.[9] The return of the z-component of the net magnetisation, M_z, to its equilibrium value, M_0, is usually a first-order process given by:

$$\frac{dM_z}{dt} = -\frac{(M_z - M_0)}{T_1}$$

(1.4)

where T_1 is the spin-lattice relaxation time constant.[17] After one T_1, M_z returns to 63% of its equilibrium value and by $5T_1$, M_z has returned to almost 100% of its equilibrium value. The T_1 values can be measured experimentally by using the inversion recovery method.[18]

(2) Transverse Relaxation

Transverse relaxation, also known as spin-spin relaxation or, somewhat erroneously, T_2 relaxation corresponds to the loss of transverse magnetisation. This results from the loss of coherence amongst the spins precessing in the

transverse plane. The decay of the x and y components of magnetisation, M_x and M_y, is also usually a first order process given by:

$$\frac{dM_x}{dt} = -\frac{M_x}{T_2} \text{ or } \frac{dM_y}{dt} = -\frac{M_y}{T_2} \qquad (1.5)$$

where T_2 is the spin-spin relaxation time constant.[17] It is important to note that the line-width at half height of the signal (in an NMR spectrum), $\Delta v_{1/2}$, depends on the T_2 of a signal as given by:

$$\Delta v_{1/2} = \frac{1}{\pi T_2^*} \qquad (1.6)$$

where

$$T_2^* = T_2 + T_{2 \text{ inhomogenous}} \qquad (1.7)$$

and $T_{2 \text{ inhomogeneous}}$ is the contribution from the inhomogeneities in the static magnetic field.[19] Therefore, a sample with short T_2 will give a broad peak and *vice-versa*. Although a rough estimate of T_2 can be obtained from the line-width at half height, for accurate measurement it is necessary to suppress the inhomogeneous broadening. This is achieved by using the 'spin-echo' technique. The simplest 'spin-echo' pulse sequence was first proposed by Hahn[20] in 1950 and later modified by Carr and Purcell[21] and Meiboom and Gill[22] to give a widely used pulse sequence named after their initials i.e. the CPMG pulse sequence.

Both T_1 and T_2 contribute to the tissue-contrast in an MRI image by affecting the signal intensity. In MRI, the protons with shorter T_1 conduce to brighter regions whereas the protons with shorter T_2 generate darker regions. This is further discussed in Section 0.

1.3 MRI Theory

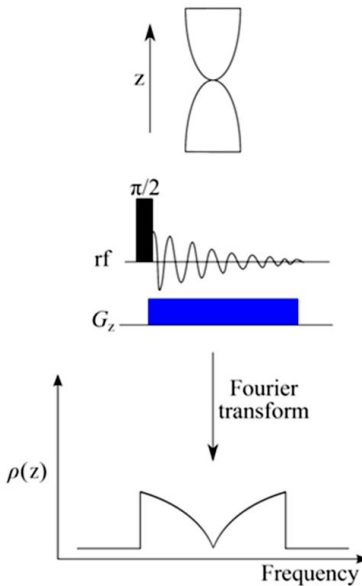## 1.3.1 Gradients - One Dimensional Imaging

Thus far, it has been discussed how an NMR spectrum can be obtained from a sample placed in a homogenous magnetic field. The next step is to consider how NMR can be used to obtain an image of the sample. Recall that the primary objective of imaging is to obtain information on the nuclear spin density, ρ, at each point in the sample (i.e., $\rho(r)$). To do so, it is necessary to spatially vary the behaviour of the nuclear spins so that spins at different positions give different signals. This can easily be achieved in NMR by varying the external magnetic field in some direction by applying a spatially well-defined magnetic gradient, G. This spatially varying magnetic field results in otherwise identical spins at different positions having different Larmor frequencies. Thus, in the presence of the magnetic gradient, the Larmor frequency becomes a function of position, r, as given by:

$$\omega(\mathbf{r}) = \gamma \mathbf{B}_0 + \gamma \mathbf{G} \cdot \mathbf{r} \qquad (1.8)$$

with the detected signal having the following form:

$$S(t) = \int \rho(\mathbf{r}) e^{i\gamma \mathbf{G} \cdot \mathbf{r} t} d\mathbf{r}. \qquad (1.9)$$

For example, an hour-glass filled with water placed in a magnetic field gradient will result in an NMR spectrum which is the projection of the distribution of spins onto the gradient direction (Figure 1.6). The amplitude of the signal at each frequency will be proportional to the number of spins in that frequency region, that is $\rho(r)$.[4, 8]

Figure 1.6 *An example of the use of a magnetic gradient to obtain a one dimensional image (i.e., $\rho(z)$) of an hourglass filled with water. The external magnetic field and the gradient are applied in the z-direction. Due to the applied gradient, the Larmor frequency becomes a function of the z-position and thus the NMR spectrum represents the distribution of the Larmor frequencies with the signal-amplitude at each frequency proportional to the number of spins in that frequency region. Thus, the image is a 1D projection of $\rho(r)$ along the direction of the gradient, i.e., $\rho(z)$.*

1.3.2 Three Dimensional Imaging - Spatial Encoding

Although the previous example is useful for understanding the effect of applying a magnetic gradient, it is important to consider that for normal (incl. medical) imaging, ρ is almost always a three dimensional (3D) quantity. And by extension of the previous example, the acquisition of a 3D image entails the application of three orthogonal gradients at appropriate junctures in the MRI pulse sequence. How these three gradients are utilized to impart spatial dependence to the nuclear spin density, a process known as spatial encoding, is discussed in the following sections.

1.3.3 Slice Selection

The first gradient is used to select a two dimensional (2D) region of interest from the sample, a process known as slice selection. This is attained by applying a spatially well-defined gradient known as the slice gradient along (say)

the z-axis throughout the sample in conjunction with a frequency selective rf pulse.[2] As depicted in Figure 1.7a, the slice gradient, G_z, varies the precession frequency of the spins linearly along the z-axis while the frequency selective rf pulse affects only those spins within the frequency range of excitation. The result is that only a limited part of the sample (the slice) is excited. Consequently, only the magnetisation contained within the slice is rotated into the transverse plane and contributes to the NMR signal. The slice thickness, Δz, is dependent on the strength of the applied gradient and the bandwidth of the frequencies incorporated into the rf pulse, $\Delta\omega_{rf}$,

$$\Delta z = \frac{\Delta\omega_{rf}}{\gamma G_z}. \tag{1.10}$$

It should be noted that regardless of the physical thickness, the selected slice is considered as a 2D object which can be manipulated to give a 1D or 2D image only. In other words, the selected slice is always considered one voxel (volume element or a '3D pixel') thick and all the information from Δz is averaged to one signal. To get a 3D image, multiple slices can be selected, imaged and stacked on each other. The position of the slice depends on the resonance frequency of the rf pulse with respect to the Larmor frequency,

$$z = \frac{\omega_{rf} - \omega_0}{\gamma G_z}. \tag{1.11}$$

The two commonly used slice selection schemes are shown in Figure 1.7b and c. The magnetisation components within the slice are dephased immediately after the application of the rf pulse which results in the destructive interference of the signals originating from the different positions of the slice.[4] Thus, a negative gradient is applied for a short period of time immediately after the use

of the rf pulse to refocus the magnetisation. Alternatively, depending on the pulse sequence, a π pulse can be used, in which case, the magnetisation refocuses automatically.
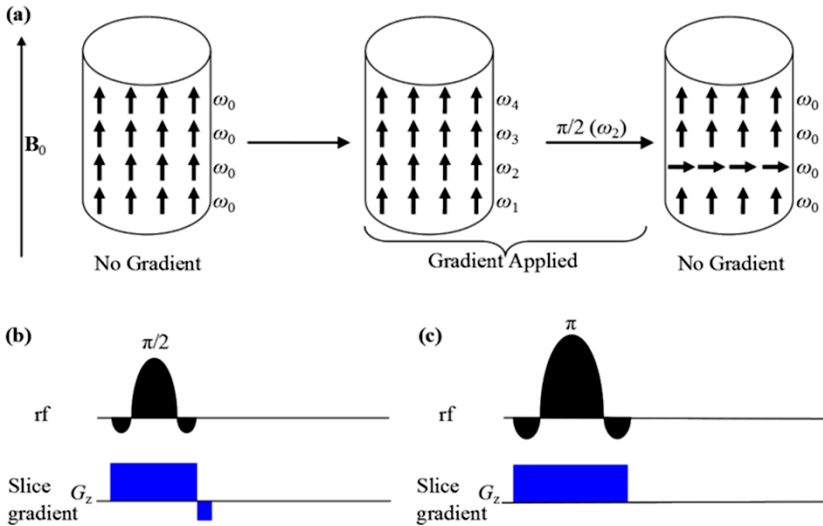
Figure 1.7 *(a) A schematic representation of the slice selection process in MRI. Before the application of a magnetic gradient, all the spins are precessing at the same frequency, ω_0. In the presence of a gradient along the direction of B_0 (i.e. z-axis), the spins at different z-positions start precessing at slightly different frequencies. If a frequency selective rf pulse is applied, only the corresponding spins are rotated into the transverse plane, thus a 'slice' is selected. The two commonly used pulse sequences are shown in (b) and (c). A short negative gradient is applied to refocus the magnetisation that had been dephased after the application of the rf pulse. Alternatively, a π pulse can be used.*

The other two gradients are used to localize the signal within the selected slice so that eventually every voxel gives a different NMR signal. The two common parameters that can be modulated to provide spatial dependence are phase and frequency as discussed in the next section.[23] For simplicity, it has been assumed that the selected slice has nine voxels and every voxel contains only one spin.
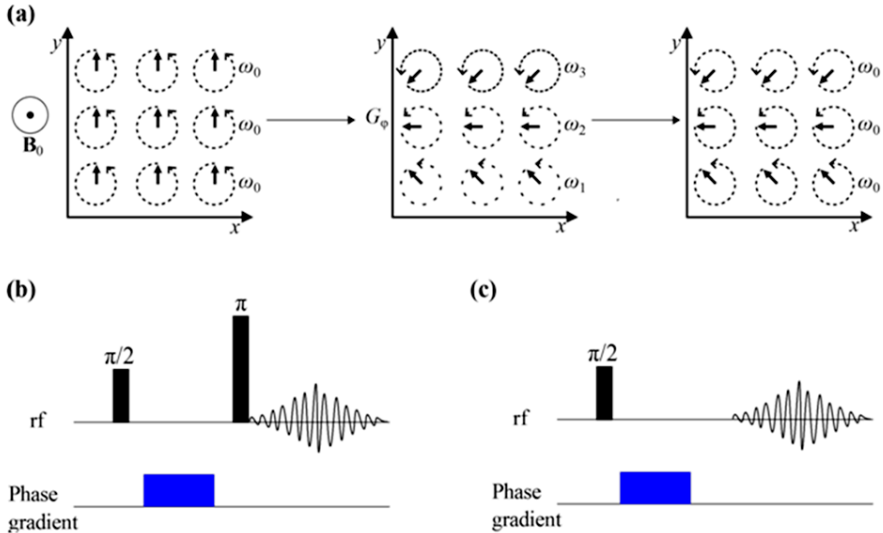
1.3.4 Phase Encoding

After the slice has been selected, all the spins within the slice are in the transverse plane. If a gradient is applied along (say) the y-axis for a fixed time t before acquiring the signal, the phase, φ, will become a function of position y as given by:

$$\phi(y) = \gamma \int_0^t (B_0 + G_\phi y) dt \qquad (1.12)$$

where G_ϕ is the phase gradient. This is because in the presence of the phase gradient, the nuclear spins along the y-axis will start precessing at slightly different frequencies and thus will have different phases at any instant. So when the gradient is stopped, although the spins retain their original precession frequency, the phase differences amongst them still remain the same. This process is known as phase encoding and is depicted in Figure 1.8a. Note that the amplitude of the signal recorded after phase encoding is inversely proportional to the strength of the applied phase gradient. The reason for this is that a stronger phase gradient results in a larger phase difference between the neighbouring spins and although this helps to resolve them better, the total signal from the spins is dephased resulting in lower amplitude.[24]

Rapid switching of the gradients generates eddy currents in the nearby conducting materials, creating a secondary source of gradients.[25, 26] This results in a distorted FID and hence the resulting image contains artifacts. A common solution for this is to use an echo sequence to allow the field distortions to dissipate before signal acquisition begins. The two common types of echo sequences are: 'spin-echo' sequences and 'gradient-echo' sequences. In the 'gradient-echo' sequence, only the gradient induced phase dispersions are refocussed in contrast to the 'spin-echo' sequence, in which phase dispersions due to the magnetic inhomogeneities and chemical shifts are refocused as well.[8,

[27, 28] The phase encoding in the 'spin-echo' and 'gradient-echo' pulse sequences are shown in Figure 1.8b and c.

Figure 1.8 *(a) An illustration of the phase encoding process in MRI. On the application of the phase gradient to the selected slice along the y-axis, the spins start precessing at different frequencies and, therefore, have different phases at any instant. After the gradient is stopped, although the spins all regain their original precession frequency (i.e., ω_0), the phase differences amongst them are retained as a function of position. (b) and (c) Phase encoding in the 'spin-echo' and 'gradient-echo' pulse sequences, respectively. The phase gradient can be applied either before or after the π pulse.*
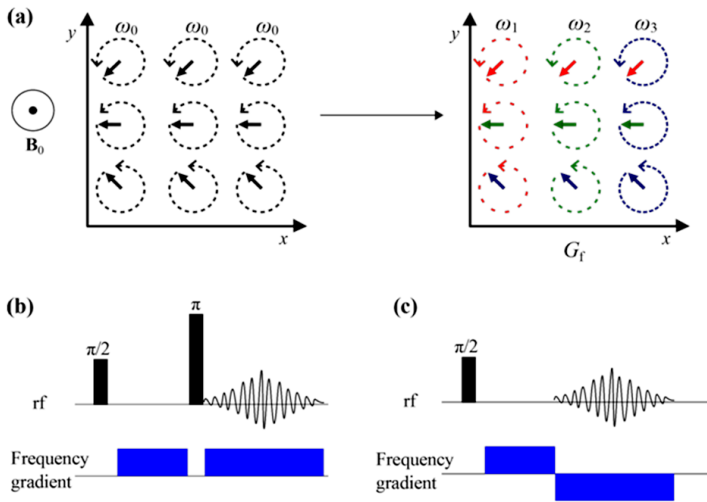
1.3.5 Frequency Encoding

Once the slice is selected and phase encoded, only one more direction needs to be resolved to get different signals from every voxel. The final gradient is applied along the x-axis while the signal is being recorded. This has the same effect as was explained in the one dimensional imaging example above i.e. the Larmor frequencies of the voxels along the x-axis become spatially dependent and Equation (1.8) can be written as:

$$\omega(\mathrm{x}) = \gamma(B_0 + G_\mathrm{f}\mathrm{x}) \tag{1.13}$$

where G_f is the frequency gradient, commonly known as the 'read' gradient.[29] This process is known as frequency encoding and is depicted in Figure 1.9a. It is clear that at the end of phase and frequency encoding, all the voxels in the selected slice are different from each other either in their phase or frequency and will, therefore, give different signals.

Putting it all together, complete basic 'spin-echo' and 'gradient-echo' 3D MRI pulse sequences are illustrated in Figure 1.10 and Figure 1.11. T_E (echo time) is the time between the application of the initial rf pulse and the acquisition of the signal and T_R (repetition time) is the time between two successive applications of a pulse sequence. Thus, T_E closely correlates with the loss of signal due to spin-spin relaxation and T_R correlates with how much longitudinal magnetisation can reform before the next pulse sequence starts. Consequently, the magnitude of the acquired signal depends strongly on both T_E and T_R. It should be noted that although in the above discussion, the slice, phase and frequency gradients have been assumed to be along the z-, y- and x-axes, respectively, in an MRI experiment, they can be applied along any three orthogonal directions.

It should be noted that whilst one frequency gradient is sufficient to resolve the voxels along the x-axis, the entire process from slice selection to signal detection needs to be repeated multiple times with different phase gradients (ranging from relative maximum negative to relative maximum positive) to completely resolve the voxels along the y-axis. The reason behind this is will become apparent in the following sections.

Figure 1.9 *(a) A pictorial representation of the frequency encoding process in MRI. After phase encoding along the y-axis, the signal is recorded in the presence of the frequency gradient along the x-axis. (b) 'spin-echo' scheme in which the sign of the magnetic gradient is effectively negated by the π pulse. In this scheme, phase dispersion due to magnetic inhomogeneities and chemical shifts and gradient-induced dispersions are refocused. (c) 'gradient-echo' scheme in which the magnetic gradients are antiphase. In this scheme, only gradient-induced dispersions are refocused.*
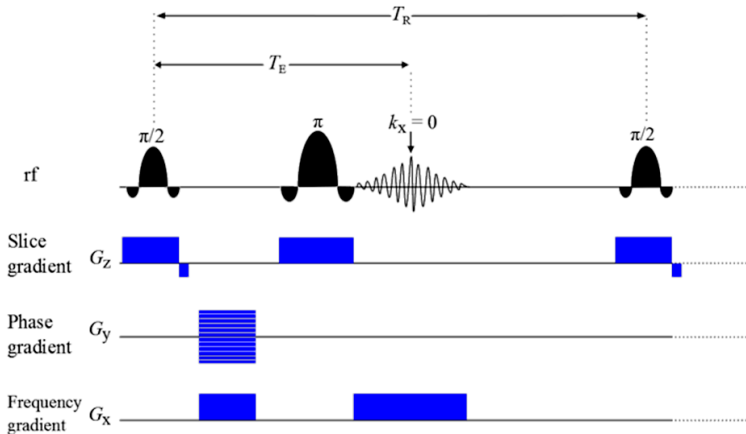

Figure 1.10 *A basic 'spin-echo' MRI pulse sequence. T_R is the repetition time and T_E is the time between the application of the initial rf pulse and the acquisition of the signal, also known as echo time. The phase gradient is drawn with equally spaced horizontal lines to indicate that its magnitude is incremented regularly when the sequence is repeated multiple times.*
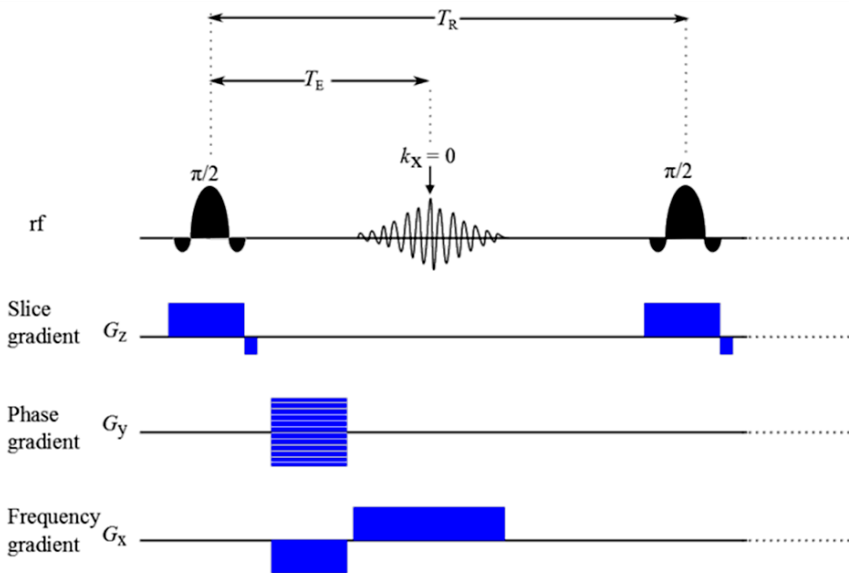
**Figure 1.11** *A basic 'gradient-echo' MRI pulse sequence.*

1.3.6 Raw Data Matrix, K - Space and Q - Space

Since a number of scans are needed to obtain enough information on one slice that a detailed 2D MRI image can be reconstructed from it, an efficient way of storing the raw data is essential. An obvious choice is to digitize the recorded echo signal by sampling the amplitudes as a function of time. This digital form of an echo is stored as a row of complex numbers. The same process is repeated for the echoes obtained with different phase gradients and these rows of complex numbers are stacked on top of each other to give a (complex) raw data matrix with the bottommost row representing the maximum negative phase gradient and the topmost row maximum positive (Figure 1.12). It is usual to display the real and imaginary parts of the complex raw data matrix as separate matrices and convert the numbers to greyscale values.
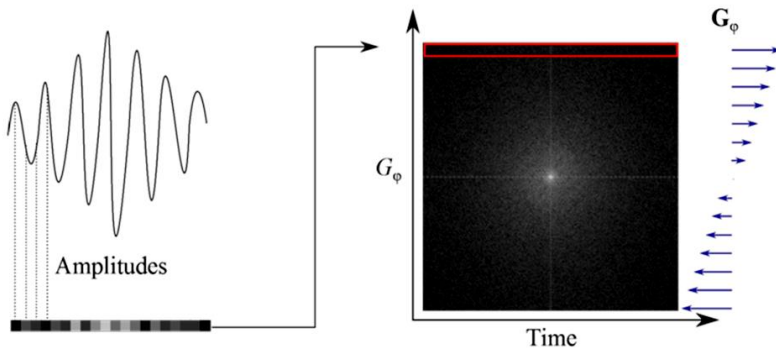
Figure 1.12 *An illustration of how the raw data is stored in MRI. The echoes are digitized by sampling their amplitudes as a function of time to give rows of complex numbers. The real (or imaginary) parts of the complex numbers can be displayed as greyscale values and stacked on top of each other to give a raw data matrix with the bottommost row representing the maximum negative phase gradient and the topmost row maximum positive.*

The raw data matrix has the dimensions of $N_\varphi \times N_f$ where N_φ is the number of phase gradients used and N_f is the number of data points recorded in the frequency encoding direction. The maximum signal is present in the centre of the raw data matrix because it corresponds to where the phase gradient was the weakest. The central region is mainly responsible for the image contrast. The outer regions of the raw data matrix have signals with low amplitudes due to strong phase gradients. These regions contain very little information about the image contrast and mainly contribute to the edge definition of the image.[2]
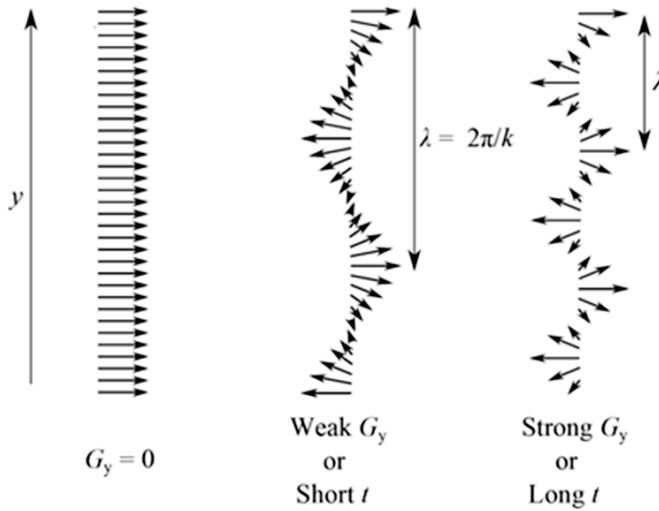
Figure 1.13 *The effect of the gradient strength and/or duration on the wave number, k. The external magnetic field is assumed to be applied along the z-axis and the spins are shown after the application of a π/2 pulse (i.e. the spins are in the transverse plane). When there is no gradient, all the spins are rotating at the same frequency and therefore, in the rotating frame of reference rotating at ω_0, the spins appear stationary with no phase difference. In the presence of a gradient, G_y, the spins start precessing with slightly different frequencies and hence a phase difference is induced, winding them into a helix of pitch $\lambda = 2\pi/k$. As the gradient strength and/or duration, t, increases, the pitch of a helix becomes smaller resulting in a shorter wavelength and correspondingly a higher k value.*

In MRI, the raw data matrix is often described in terms of wave numbers. A wave number, k, is the number of wavelengths per 2π units of distance i.e. $k = 2\pi/\lambda$ (rad m^{-1}), where λ is the wavelength. Analogous to frequency which is the number of oscillation per unit time, k is also called the spatial frequency. The spatial frequency is proportional to the gradient strength and the duration of the gradient. This is because a higher gradient strength gives a greater frequency differential and a longer duration gradient gives a greater phase differential which results in shorter wavelengths and correspondingly larger k-values (Figure 1.13).

Thus, the *k*-values along the phase and frequency encoding axes can be written as:

$$
\begin{aligned}
k_{\mathrm{y}} &= \gamma G_{\varphi} t \text{ and} \\
k_{\mathrm{x}} &= \gamma G_{\mathrm{f}} t,
\end{aligned}
\tag{1.14}
$$

respectively. Also, after making the adjustments to Equation (1.9), the acquired signal (echo) can be written as a function of *k*,

$$
\begin{aligned}
S(k_{\mathrm{y}}) &= \int \rho(\mathrm{y}) \mathrm{e}^{i2\pi k_{\mathrm{y}} \mathrm{y}} d\mathrm{y}, \\
S(k_{\mathrm{x}}) &= \int \rho(\mathrm{x}) \mathrm{e}^{i2\pi k_{\mathrm{x}} \mathrm{x}} d\mathrm{x}.
\end{aligned}
\tag{1.15}
$$

Combining these equations, the total signal from the selected slice can be written as:

$$
S(k_{\mathrm{x}}, k_{\mathrm{y}}) = \iint \rho(\mathrm{x}, \mathrm{y}) \mathrm{e}^{i2\pi(k_{\mathrm{x}} \mathrm{x} + k_{\mathrm{y}} \mathrm{y})} d\mathrm{x} d\mathrm{y}.
\tag{1.16}
$$

Consequently, the raw data matrix can be edited to replace 'time' with 'k_{x}' along the x-axis and 'G_{φ}' with 'k_{y}' along the y-axis. In other words, each point along the frequency encoding axis now corresponds to the k_{x} value and along the phase encoding axis to the k_{y} value (Figure 1.14). This description of the raw data matrix is known as the k-space formalism; and the raw data matrix itself is in k-space. The k-space formalism is a convenient method for describing the different ways of acquiring data, as explained in Section 0.

$$k_y = \gamma G_\varphi t$$
$$k_x = \gamma G_t t$$

Raw Data Matrix

k-space
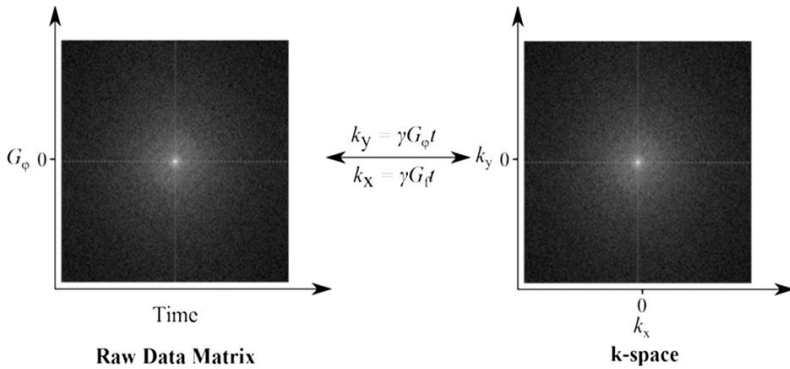
Figure 1.14 *Two descriptions of the raw data storage. Although both the matrices contain the same data, it is convenient to describe the signal as a function of the spatial frequency, k, as it makes it easier to describe different methods of acquiring data using various MRI pulse sequences.*

Similar to k-space which is conjugate to r-space (i.e., the laboratory frame), it is possible to define q-space which is conjugate to displacement $r_0 - r_1$. Obtaining q-space data allows construction of the nuclear spin self-correlation function, $P_s(r_1 - r_0, \Delta)$, which gives the conditional probability that a spin has been displaced by $r_0 - r_1$ during time Δ.[30] Nuclear spin displacement over a given period Δ may be tracked by using a pair of magnetic gradient pulses sandwiching a $180\,^\circ$ rf pulse with the leading edges of the gradient pulses separated by Δ. q is defined as:

$$\mathbf{q} = \frac{\gamma \mathbf{g} \delta}{2\pi},\tag{1.17}$$

where δ is the duration of the gradient pulses and g is a constant gradient giving a linear variation in the *z*-component of the magnetisation.

Evidently q has dimensions of inverse distance or m^{-1} in SI units and is analogous to k. q-space is useful for measuring both coherent motion (flow) and incoherent motion (diffusion) by measurement of the phase shift and attenuation

of the magnetisation helices using the pulse gradient spin-echo pulse sequence, respectively.[31] The first gradient winds the magnetisation into a helix; the rf pulse changes the chirality of the helix so that the next gradient pulse will unwind the helix. The helix persists for a duration Δ during which it is affected by flow and diffusion. Diffusion causes the magnetisation helix to attenuate as nuclear spins from one part of the helix diffuse into other parts causing the phases to cancel. If there is flow along the axis of the helix the whole helix will move and there will be an effective phase shift. After unwinding the helix with the second gradient pulse, the attenuation and phase shift persist although the magnetisation is now back in spatial coherence. Information on diffusion and flow can now be acquired simply by acquiring and analyzing the FID (for a variety of gradient strengths). A detailed calculation of the effects of diffusion and flow reveal that the signal will be affected according to:

$$S(\mathbf{g}) = S(0)\exp\left(-\gamma^2\delta^2\mathbf{g}\cdot\mathbf{D}\cdot\mathbf{g}(\Delta-\delta/3)-i\gamma\delta\mathbf{g}\cdot\mathbf{v}\Delta\right), \qquad (1.18)$$

where D is the diffusion tensor and v is the flow velocity. The first term in the exponent of Equation (1.18) gives the attenuation of the signal resulting from diffusion. Note that the greater the diffusion coefficient the greater the attenuation. Attenuation is also greater for larger diffusion time Δ and more powerful gradient pulses. By holding δ and Δ constant and measuring the attenuation for different g the diffusion tensor (or diffusion coefficient for isotropic diffusion) can be constructed. The second term in Equation (1.18) gives the phase shift of the signal which is a function of the velocity of the fluid parallel to the applied gradients. Measurements of phase shift for a variety of gradient strengths provide information on laminar fluid flow characteristics.

1.3.7 Image Reconstruction

In this section, reconstruction of an MRI image and the different ways of acquiring raw data are discussed using the k-space formalism.

Recalling that an MRI image is essentially the nuclear spin density in 'real space' (i.e. $\rho(x, y)$) and realizing from Equation (1.16) that the signal in k-space is in fact an inverse Fourier transform of the nuclear spin density in 'real space', it is evident that an MRI image of the selected slice can be reconstructed by the 2D Fourier transform of the signal in k-space (Figure 1.15) as given by:

$$\rho(x, y) = \int\int S(k_x, k_y) e^{-i2\pi(k_x x + k_y y)} dk_x dk_y. \tag{1.19}$$
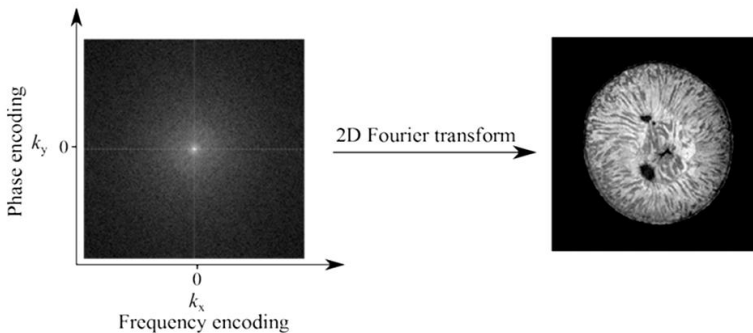
Figure 1.15 *An MRI image can be reconstructed by applying a 2D Fourier transform to the k-space data. Note only the magnitude of the k-space data is shown here (as k-space data from MRI is inherently complex).*

Note that even though k-space stores all the data that is required to construct an image, it is usually hard to predict what the final image will look like after the 2D Fourier transform of the k-space data. This is exemplified in Figure 1.16 by simulating some basic shapes and their k-space images.
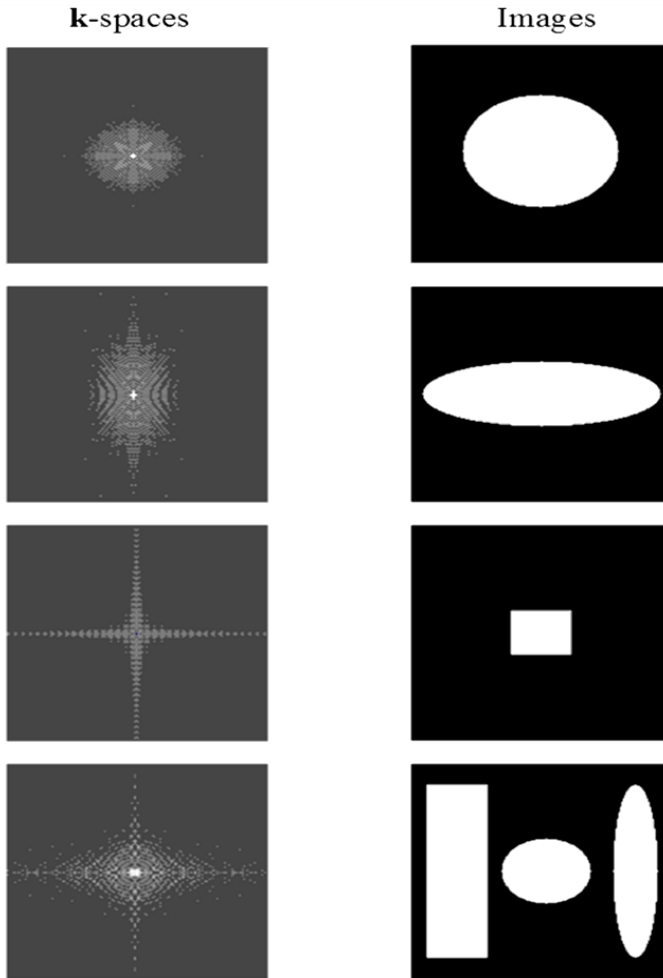
k-spaces   **Images**

Figure 1.16 A few simulated k-spaces and their corresponding images. For basic symmetrical shapes (circle, ellipse and square), it is possible to predict what the final image will look like from its k-space. But even for slightly complicated shapes (bottom most), the k-space becomes non indicative of the final image.

It is important to acquire a detailed k-space data set to obtain a good quality image. In fact, the resolution of the image depends on the number of points in k-space. For example, a 128×256 k-space data set will result in an image with 128 pixels along the phase encoding axis and 256 pixels along the frequency encoding axis. So, the higher the number of points in k-space the better the image resolution. However, this requires a lot of time which is of prime importance in MRI. So, various pulse sequences have been designed to more

efficiently acquire sufficient k-space data. These sequences use different combinations of the phase and frequency gradients to map data in k-space in a quicker yet efficient manner. The geometry in which the k-space data is acquired is called a 'raster'. Two common examples are the Cartesian raster sampling and polar raster sampling.[4, 32]
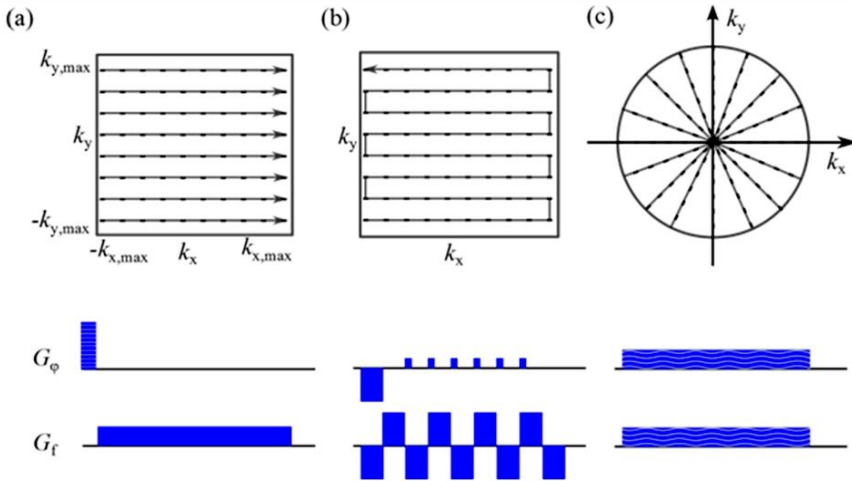
Figure 1.17 *Examples of different ways of acquiring k-space data in a geometry plane known as a 'raster'. Cartesian rasters can be obtained by 2D Fourier transform imaging pulse sequences such as a spin- or gradient-echo (a) and echo planar imaging pulse sequence (b). Projection reconstruction imaging pulse sequences, such as filtered back projection reconstruction pulse sequence (c), acquire k-space in polar rasters.*

The imaging process in which the selected slice is sampled in a Cartesian raster is called Fourier imaging. For example, the spin-echo and gradient-echo pulse sequences (Figure 1.10 and Figure 1.11) acquire the raw data in the Cartesian raster in a linear fashion as shown in Figure 1.17a. The stepping of the phase gradient from the most negative to most positive value in fixed intervals traverses k-space from $-k_{y,max}$ to $k_{y,max}$ and for each phase gradient, the applied frequency gradient samples the points from $-k_{x,max}$ to $k_{x,max}$. Another

example of the k-space traversal in the Cartesian raster is shown in Figure 1.17b by using an echo planar imaging pulse sequence.[33]

If k-space is traversed in a polar raster, the imaging process is called projection reconstruction imaging.[34] For example, the filtered back projection reconstruction pulse sequence and its polar raster are shown in Figure 1.17c. In this pulse sequence, the phase and frequency gradients are applied simultaneously following the sine and cosine relationships respectively, which is equivalent to applying a net gradient, $G = \sqrt{G_\varphi^2 + G_f^2}$ rotating around the polar angle, $\tan \theta = G_\varphi/G_f$.[4, 35]

1.4 MRI Contrast

Contrast between different tissue types is of utmost importance for every imaging modality. In MRI, this contrast results from spatial variations in the spin density of the observed nucleus and the physical and chemical environment of the nucleus.[32] These sources of contrast can be broadly classified into two categories: endogenous and exogenous. These are briefly discussed below.

1.4.1 Endogenous Sources

Important endogenous sources of contrast in MRI include spin density, relaxation times of the observed nuclei, magnetic susceptibility, diffusion and flow. Spin density contrast provides contrast on the basis of the number of spins (e.g. water protons) present in a voxel which differs across the tissue types. Since M_Z of each voxel is composed of the individual spins within that voxel, this variation in spin density affects the signal intensity in an MRI image. For example, in ^{1}H MRI, blood will appear brighter than muscles which in turn will appear much brighter than bones. Also, the molecular dynamics within the

tissue can affect T_1 and T_2 of the water protons. Therefore, the water protons present in different tissue types will have different relaxation times which again affect the net magnetisation and thus the signal intensity. By carefully engineering the imaging pulse sequence, it is also possible to obtain dynamic contrast in MRI due to diffusion and flow. An example of such pulse sequences is diffusion tensor imaging which can be used to probe the transport properties within a tissue e.g. diffusion of water in brain tissue (note that in such imaging techniques, the q-space formalism is used as well as the k-space formalism as explained in the section above).[36] In MRI, it is possible to set the experimental parameters like the repetition and echo time to enhance or diminish the contrast based on one contrast factor. For example, in T_1-weighted imaging, T_2 effects can be minimised by setting the echo time such that $T_E \ll T_2$ (more details on this can be found in the literature[37]). However, regardless of the parameters selected, the resulting image will always depend on other contrast factors to some extent.

The chemical environment of the observed nuclei can also induce contrast in MRI by affecting observables like chemical shift, spin-spin coupling constants and inter nuclear dipolar interactions. As an example, chemical shift imaging can be used to explore an extra dimension in the imaging experiment by probing the frequency spread due to different chemical shifts in a sample with two different chemical species (e.g. water and fat in biological systems).[38, 39] Due to this extra dimension, in its ultimate form, chemical shift imaging is sometimes referred to as 'four dimensional imaging' (three from the spatial axes and one from the chemical shift).[40] There are many other forms of contrast in MRI such as magnetic susceptibility,[41] temperature[42] and blood oxygenation level dependence (BOLD),[43, 44] details on which can be found elsewhere.

1.4.2 Exogenous Sources - Contrast Agents

The naturally occurring contrast between tissues is often insufficient to distinguish between diseased and healthy tissue especially in cases such as cancer. This gives rise to the need of contrast enhancement which is achieved by the use of chemicals known as contrast enhancement agents or contrast agents (CAs). In MRI, CAs modulate the relaxation times of water protons inside tissue to provide enhanced image contrast. The efficiency of a CA is measured in terms of its relaxivity (r_1 or r_2), which is defined as the change in the relaxation rate of water protons upon the addition of a CA, normalised to its concentration:

$$r_i = \frac{\Delta 1/T_i}{[CA]}; \quad i = 1, 2. \tag{1.20}$$

All CAs increase both r_1 and r_2 to varying degrees, depending on whether they are categorised as positive ($r_2/r_1 = 1$–2) or negative (r_2/r_1 as high as 10 or more) CAs.[45] Negative or T_2 CAs are mostly constructed from superparamagnetic iron oxide (SPIO) and induce negative contrast by decreasing the signal intensity of the affected water protons.[46, 47] Positive or T_1 CAs are mainly comprised of paramagnetic metal ions such as Gd (III) chelated to multi-dentate ligands. These CAs induce positive contrast by increasing the signal intensity of the affected water protons and are, therefore, preferred over the negative CAs by MRI practitioners.[48, 49] There have also been some studies on ^{19}F-based CAs, which can be detected directly by ^{19}F MRI.[50, 51]

1.5 Applications

MRI has numerous applications in a vast variety of areas. However, unsurprisingly biological studies were and still remain the major application of

MRI. Due to its non-invasive and safe nature, MRI has been used to explore systems that were previously inaccessible. Also with the advancement of technology, clinical MRI scanners are constantly moving to higher fields to provide better image resolution, thus enabling clinicians to detect minor abnormalities which could not have been seen before. Some of the many clinical applications of MRI include the anatomical and physiological studies of embryo,[52] heart,[53, 54] kidney[55] and brain.[56, 57] With the use of CAs, MRI has also proven very efficient in detecting tumours.[58] Moreover, MRI has been used in plant studies to examine various aspects such as water flow characteristics in the phloem and xylem,[59, 60] freezing behaviour in plants[61] and plant histochemistry.[62]

MRI is also a distinctive tool to study the distribution of species and phase transitions in chemical systems. Some examples include the spatial localization of hydrogen in the H-Pd system,[63] observation of chromatographic bands of gadolinium chelates[64] and 3D imaging of $^1H_2$, $^2H_2$ and their isotopic mixtures.[65] Apart from these, there are many more applications ranging from food science,[66] polymers[67] to petrochemicals[68] which are outside the scope of this chapter.

References

[1]   P. C. Lauterbur, *Nature*, 1973, 242, 190-191.

[2]   M. A. Brown and R. C. Semelka, *MRI: basic principles and applications*, Wiley-Blackwell, New Jersey, 2010.

[3]   M. E. Haacke, R. W. Brown, M. R. Thompson and R. Venkatesan, *Magnetic resonance imaging: physical principles and sequence design*, Wiley-Liss, New York, 1999.

[4]   W. S. Price, in *Annu. Rep. NMR Spectrosc.*, ed. G. A. Webb, Academic Press, 1998, pp. 139-216.

[5]   P. T. Callaghan, *Translational dynamics and magnetic resonance*, Oxford, Oxford, 2011.

[6]   P. Storey, in *Magnetic resonance imaging: methods and biological applications*, ed. P. V. Prasad, Humana Press, New Jersey, 2006.

[7]   P. T. Callaghan, *Principles of nuclear magnetic resonance microscopy*, Clarendon Press, Oxford, 1991.

[8]   S. L. Talagala and I. J. Lowe, *Concepts Magn. Res.*, 1991, 3, 145-159.

[9]   M. H. Levitt, *Spin dynamics: basics of nuclear magnetic resonance*, Wiley, New York, 2008.

[10]   C. Westbrook, C. K. Roth and J. Talbot, *MRI in practice*, Blackwell, Oxford, 2005.

[11]   J. Keeler, *Understanding NMR spectroscopy*, Wiley, Chichester, 2010.

[12]   J. W. Akitt and B. E. Mann, *NMR and chemistry: an introduction to modern NMR spectroscopy*, Stanley Thornes, New York, 2000.

[13]   F. A. Bovey, P. A. Mirau and H. Gutowsky, *Nuclear magnetic resonance spectroscopy*, Academic Press, 1988.

[14]   M. E. Halse, A. Coy, R. Dykstra, C. Eccles, M. Hunter, R. Ward and P. T. Callaghan, *J. Magn. Reson.*, 2006, 182, 75-83.

[15]   J. C. Hoch and A. S. Stern, *NMR data processing*, Wiley, New York, 1996.

[16]   R. R. Ernst and W. A. Anderson, *Rev. Sci. Instrum.*, 1966, 37, 93-102.

[17]   J. H. Nelson, *Nuclear magnetic resonance spectroscopy*, Prentice Hall, New Jersey, 2003.

[18]   R. L. Vold, J. S. Waugh, M. P. Klein and D. E. Phelps, *J. Chem. Phys.*, 1968, 48, 3831.

[19]   J. Kowalewski and L. Mäler, *Nuclear spin relaxation in liquids: theory, experiments, and applications*, Taylor & Francis, New York, 2006.

[20]   E. L. Hahn, *Phys. Rev.*, 1950, 80, 580.

[21]   H. Y. Carr and E. M. Purcell, *Phys. Rev.*, 1954, 94, 630.

[22] S. Meiboom and D. Gill, *Rev. Sci. Instrum.*, 1958, 29, 688-691.

[23] S. A. Huettel, A. W. Song and G. McCarthy, *Functional magnetic resonance imaging*, Sinauer, Massachusetts, 2004.

[24] D. G. Mitchell and M. S. Cohen, *MRI principles*, Saunders, Pennsylvania, 2004.

[25] S. Robertson, D. G. Hughes, Q. Liu and P. S. Allen, *Magn. Reson. Med.*, 1992, 25, 158-166.

[26] M. Burl and I. R. Young, in *Encyclopedia of Nuclear Magnetic Resonance*, eds. D. M. Grant and R. K. Harris, Wiley, New York, 1996, pp. 1841-1846.

[27] J. Hennig, *Concepts Magn. Res.*, 1991, 3, 179-192.

[28] J. Hennig, *Concepts Magn. Res.*, 1991, 3, 125-143.

[29] R. Mulkern, *Concepts Magn. Res.*, 1992, 4, 307-325.

[30] P. T. Callaghan, C. D. Eccles and Y. Xia, *J. Phys. E: Sci. Intrum.*, 1988, 21, 820.

[31] W. S. Price, *Concepts Magn. Res.*, 1997, 9, 299-336.

[32] Y. Xia, *Concepts Magn. Res.*, 1995, 8, 205-225.

[33] M. K. Stehling, R. Turner and P. Mansfield, *Science*, 1991, 254, 43-50.

[34] G. H. Glover and J. M. Pauly, in *Encyclopedia of Nuclear Magnetic Resonance*, eds. D. M. Grant and R. K. Harris, Wiley, New York, 1996, pp. 3772-3778.

[35] G. H. Glover and J. M. Pauly, *Magn. Reson. Med.*, 1992, 28, 275-289.

[36] P. J. Basser, J. Mattiello and D. LeBihan, *Biophys. J.*, 1994, 66, 259-267.

[37] M. L. Lipton, in *Totally accessible MRI*, Springer, New York, 2008, pp. 38-46.

[38] L. Brateman, *Am. J. Roentgenol.*, 1986, 146, 971-980.

[39] P. E. Sijens, M. J. Van Den Bent, P. J. C. M. Nowak, P. van Dijk and M. Oudkerk, *Magn. Reson. Med.*, 1997, 37, 222-225.

[40] A. Maudsley, S. Hilal, W. Perman and H. Simon, *J. Magn. Reson.*, 1983, 51, 147-152.

[41] J. L. Boxerman, L. M. Hamberg, B. R. Rosen and R. M. Weisskoff, *Magn. Reson. Med.*, 1995, 34, 555-566.

[42]   D. L. Parker, V. Smith, P. Sheldon, L. E. Crooks and L. Fussell, *Med. Phys.*, 1983, 10, 321.

[43]   S. Ogawa, T. M. Lee, A. R. Kay and D. W. Tank, *Proc. Natl. Acad. Sci. U. S. A.*, 1990, 87, 9868-9872.

[44]   K. R. Thulborn, J. C. Waterton, P. M. Matthews and G. K. Radda, *Biochim. Biophys. Acta*, 1982, 714, 265-270.

[45]   P. Caravan, J. J. Ellison, T. J. McMurry and R. B. Lauffer, *Chem. Rev.*, 1999, 99, 2293-2352.

[46]   J. W. M. Bulte and D. L. Kraitchman, *NMR Biomed.*, 2004, 17, 484-499.

[47]   Y. X. Wang, S. Hussain and G. Krestin, *Eur. Radiol.*, 2001, 11, 2319-2331.

[48]   R. B. Lauffer, *Chem. Rev.*, 1987, 87, 901-927.

[49]   A. Accardo, D. Tesauro, L. Aloj, C. Pedone and G. Morelli, *Coord. Chem. Rev.*, 2009, 253, 2193-2213.

[50]   H. Peng, I. Blakey, B. Dargaville, F. Rasoul, S. Rose and A. K. Whittaker, *Biomacromolecules*, 2009, 10, 374-381.

[51]   R. Díaz-López, N. Tsapis and E. Fattal, *Pharm. Res.*, 2010, 27, 1-16.

[52]   D. Prayer, ed., *Fetal MRI*, Springer, New York, 2011.

[53]   C. Higgins, *Am. J. Roentgenol.*, 1988, 151, 239-248.

[54]   C. B. Higgins and A. d. Roos, eds., *MRI and CT of the cardiovascular system*, Lippincott Williams and Wilkins, Pennsylvania, 2006.

[55]   P. V. Prasad, in *Magnetic resonance imaging: methods and biological applications*, ed. P. V. Prasad, Humana Press, New Jersey, 2006.

[56]   L. Cecconi, A. Pompili, F. Caroli and E. Squillaci, in *MRI atlas of central nervous system tumors*, Springer, 1992, pp. 33-83.

[57]   H. M. Duvernoy and B. Parratte, *The human brain: surface, three-dimensional sectional anatomy with MRI, and blood supply*, Springer Vienna, 1999.

[58]   T. Barrett, H. Kobayashi, M. Brechbiel and P. L. Choyke, *Eur. J. Radiol.*, 2006, 60, 353-366.

[59]   N. M. Holbrook, E. T. Ahrens, M. J. Burns and M. A. Zwieniecki, *Plant Physiol.*, 2001, 126, 27-31.

[60] C. W. Windt, F. J. Vergeldt, P. A. De Jager and H. Van As, *Plant Cell Environ.*, 2006, 29, 1715-1729.

[61] H. Ide, W. S. Price, Y. Arata and M. Ishikawa, *Tree Physiol.*, 1998, 18, 451-458.

[62] V. Sarafis, H. Rumpel, J. Pope and W. Kuhn, *Protoplasma*, 1990, 159, 70-73.

[63] E. W. McFarland and D. Lee, *J. Magn. Reson. A*, 1993, 102, 231-234.

[64] U. Tallarek, E. Baumeister, K. Albert, E. Bayer and G. Guiochon, *J. Chromatogr. A*, 1995, 696, 1-18.

[65] J. M. Moore, P. Blumler, M. H. Sherwood, C. G. Wade, G. W. Collins and E. R. Mapoles, *J. Magn. Reson. A*, 1994, 110, 248-251.

[66] B. Hills, *Magnetic resonance imaging in food science*, Wiley New York, 1998.

[67] M. Maryanski, R. Schulz, G. Ibbott, J. Gatenby, J. Xie, D. Horton and J. Gore, *Phys. Med. Biol.*, 1994, 39, 1437.

[68] W. P. Rothwell and H. Vinegar, *Appl. Opt.*, 1985, 24, 3969-3972.